ACS Sustainable Chemistry & Engineering

pubs.acs.org/journal/ascecg

Open Access

This article is licensed under CC-BY 4.0

Research Article

Alkylpolyglucoside-Stabilized Oleic Acid Nanodroplets as a Sustainable Platform for the Aqueous Dispersion of Essential Oil Compounds

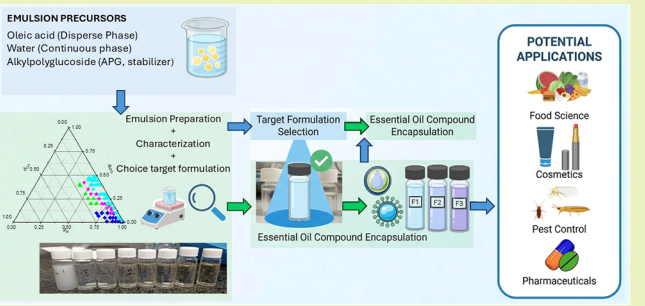
Laura Fernández-Peña, Emilie Larguier, Solange d'Aligny, Alejandro Toledo-Sánchez, Paula Porawski-González, Alejandro Lucia, Chaïma Amara, Francisco Ortega, Ramón G. Rubio, and Eduardo Guzmán*

Cite This: https://doi.org/10.1021/acssuschemeng.5c13845

Read Online

ACCESS | Metrics & More | Article Recommendations

ABSTRACT: The encapsulation of hydrophobic bioactive molecules, such as essential oil compounds (EOCs), in aqueous nanodispersions is critical for enhancing their solubility, stability, and applicability across diverse industries. This study examines the formulation of oleic acid nanodroplets stabilized by a biobased alkylpolyglucoside (APG), without the need for auxiliary cosurfactants. In this system, oleic acid simultaneously provides the oil core and contributes to interfacial charging, enabling the nanodroplets to act as efficient carriers for thymol and carvacrol. In contrast to conventional formulations requiring cosurfactants, this work presents a simplified and greener approach. A pseudoternary phase diagram defined the regions of stable dispersion formation, confirming the feasibility of a one-surfactant-only system. Dynamic light scattering confirmed a monomodal size distribution (10−15 nm), whereas fluorescence spectroscopy revealed up to three distinct chemical environments for the EOCs within the droplets. Crucially, the system's stability is governed by the pH-dependent dissociation of oleic acid at the interface, as elucidated by conductivity and pH measurements. The results demonstrate that increasing EOC concentration leads to droplet growth, which may destabilize dispersions, highlighting the need for compositional optimization. This APG/oleic acid platform provides a scalable, eco-friendly alternative for delivering poorly soluble bioactives, aligning with the principles of sustainable chemistry and reducing the environmental footprint of essential oil formulations.



KEYWORDS: *colloidal dispersions, emulsions, essential oil compounds, nanodroplets, solubilization*

INTRODUCTION

Essential oils and their individual constituents form a diverse family of bioactive compounds with a broad range of technical and biological applications.[1−6] Their multifunctional properties, such as antimicrobial, antifungal, antioxidant, and insecticidal activities, have been harnessed in food preservation,[7] pest control,[8−10] and cosmetic formulations.[1] Despite these advantages, the practical use of essential oils is hindered by their intrinsic volatility, poor water solubility, and thermal and chemical instability.[11,12] These limitations, which include photodegradation, hydrolysis, oxidation, and thermal decomposition, necessitate innovative strategies to preserve their bioactivity.[13] Among the various approaches, encapsulation in nanoscale carriers, particularly oil-in-water (O/W) emulsion-like dispersions, has emerged as a promising solution, offering enhanced bioavailability and stability for poorly water-soluble compounds.[2,14−16] Moreover, the high surface area of nanodroplets facilitates improved interactions with target substrates, thereby increasing formulation efficiency.[17−20]

This work investigates the application of oleic acid nanodroplets, stabilized by an alkylpolyglucoside (APG), as a delivery vehicle for two isomeric essential oil compounds (EOCs), namely thymol and carvacrol. These natural monoterpenoids, derived from *p*-cymene and commonly found in extracts from plants of the *Lamiaceae* family,[21,22] are recognized for their potent antimicrobial effects[23] as well as antitumoral[24] and antihypertensive activities.[25]

Due to their hydrophobic nature, both thymol and carvacrol require an appropriate environment to enhance their aqueous solubility, bioavailability, and stability, challenges that can be addressed by encapsulation in oleic acid nanodroplets.[26−28]

Received: December 19, 2025
Revised: March 3, 2026
Accepted: March 4, 2026

Downloaded via 190.7.229.70 on March 12, 2026 at 13:46:59 (UTC).
See https://pubs.acs.org/sharingguidelines for options on how to legitimately share published articles.

ACS Publications

© XXXX The Authors. Published by American Chemical Society

We systematically investigate the interplay between oleic acid, APG, and essential oil compounds (EOCs) to elucidate the key parameters governing droplet stability and solubilization. In this context, the main goal of our study is to understand how thymol and carvacrol are encapsulated by oleic acid nanodroplets. For this purpose, we evaluate the pseudoternary phase diagram to define the compositional range that guarantees the formation of stable nanodroplets, highlighting the complex interplay between oleic acid and APG concentrations. Dynamic light scattering (DLS) is employed to analyze droplet size distributions, while fluorescence spectroscopy provides insights into the chemical microenvironments of the two EOCs within the droplets. Collectively, these studies advance our understanding of the encapsulation mechanisms of essential oil compounds and identify optimal conditions for achieving stable dispersions. Importantly, our findings reveal that APG, a nonionic biosurfactant recognized for its excellent emulsifying performance, biocompatibility, and low toxicity, stabilizes oleic acid nanodroplets without auxiliary cosurfactants (e.g., ethanol/lecithin[29−31]), where OA acts dually as oil phase and interfacial costabilizer. This yields cosurfactant-free dispersions. Although previous studies have encapsulated essential oil compounds in oleic-acid−based nanodroplets using alkylpolyglucosides, they typically incorporate additional stabilizing agents such as ethanol or lecithin to ensure droplet stability..[29−31] Avoiding these additional components not only simplifies the formulation but also reduces its environmental impact, as organic solvents contribute to volatile organic compound emissions and require energy-intensive purification,[32] while lecithin-based systems involve extra processing steps and variable life-cycle impacts.[33] Relying exclusively on APG therefore lowers the overall chemical footprint and aligns with green-chemistry principles that favor streamlined compositions, improved biodegradability, and reduced waste generation.[34,35] It is worth mentioning that this work should be considered as a proof-of-concept study. For this reason, analytical-grade thymol, carvacrol, and oleic acid were employed to ensure well-controlled composition and reproducible colloidal behavior. However, both thymol and carvacrol are routinely obtained from plant essential oils, and oleic acid can increasingly be sourced from residual or waste lipid streams.[36−38] On the other hand, while analytical-grade oleic acid ensures compositional control (≥99% C18:1), waste lipid streams from spent cooking oils, animal rendering, or algal biomass typically contain 60−80% C18:1 alongside saturates (C16:0, C18:0), oxidized triglycerides, and trace phospholipids.[39] These impurities may modify the pseudoternary diagram by (i) reducing effective HLB through saturated chain incorporation, (ii) promoting partial coalescence via oxidation products, and (iii) altering interfacial rheology via phospholipids.[40] Integrating biobased and waste-derived feedstocks into the current APG/oleic-acid platform remains challenging; however, successful incorporation could significantly enhance the sustainability of these formulations within a circular-economy framework.

This research contributes to the development of efficient delivery systems for poorly water-soluble bioactive compounds, with potential benefits across the pharmaceutical, food, and cosmetic industries.[41−43] In particular, the potential application of the proposed formulations in food preservation stands out as particularly promising.[44,45] It is well established that thymol and carvacrol exhibit strong antibacterial activity against a wide range of foodborne pathogens, with reported minimum inhibitory concentrations (MICs) typically in the 150−400 mg/L range, depending on the microorganism and experimental conditions.[46−48] Recent studies further show that incorporating these phenolic compounds into nanoemulsions or related nanocarriers can maintain or even enhance their antimicrobial efficacy, owing to improved aqueous dispersion, protection against volatilization and oxidation, and facilitated interaction with microbial cell membranes.[49] In this context, the APG−oleic acid nanodroplets developed in this work align well with these requirements, offering a simple and fully biobased platform capable of dispersing hydrophobic essential oil components in water without the need for cosurfactants or organic solvents. This makes food preservation an especially compelling application for the sustainable nanodroplet system proposed here.

MATERIALS AND METHODS

Chemicals

Oleic acid, with a purity of >99%, was obtained from Sigma-Aldrich (Darmstadt, Germany). Similarly, thymol (2-isopropyl-5-methylphenol) and carvacrol (5-isopropyl-2-methylphenol), with a purity of >98.5%, were also acquired from Sigma-Aldrich (Darmstadt, Germany). To stabilize the nanodroplets in an aqueous medium, an alkylpolyglucoside (APG), supplied by Safic-Alcan (Barcelona, Spain), was employed. This APG, designated with the commercial name Oramix CG-110, is supplied as an aqueous dispersion with 60% in weight of active matter, which contains 50:50 molar mixture of caprylyl glucoside and capryl glucoside. Oramix CG-110 was selected due to its HLB (hydrophilic−lipophilic balance) value above 10 (∼13−14),[50] which provides a satisfactory balance for stabilizing oleic-acid nanodroplets without the need for cosurfactants.[51,52] As a short-chain nonionic alkyl polyglucoside, Caprylyl/Capryl Glucoside exhibits rapid interfacial adsorption and efficient interfacial tension reduction, favoring the formation of high-curvature micellar and emulsion structures. This behavior contrasts with longer-chain APGs (C12−C16, such as lauryl or myristyl glucosides), whose lower HLB values and stronger lipophilic interactions promote lamellar or liquid-crystalline phases that typically require additional stabilizers to achieve comparable O/W emulsification performance.[53−55] The superior interfacial activity of C8−C10 APGs aligns with established structure−performance relationships demonstrating that shorter alkyl chains enhance spontaneous emulsification, droplet size reduction, and kinetic stability in systems containing low-polarity fatty acids like oleic acid.[53] Recent studies have furtherly confirmed the ability of APGs to modulate interfacial structures and improve the physical stability of complex colloidal formulations, supporting the preferential use of C8−C10 glucosides in cosmetic nanoemulsions where mildness and efficient O/W stabilization are required.[53,55,56] It is worth noting that no cosurfactants were used in order to minimize the environmental impact of the formulation. Avoiding these additives reduces solvent use, lowers Volatile Organic Compound emissions, and eliminates additional processing steps associated with cosurfactant purification, thereby improving the overall sustainability of the system.

The dispersions were prepared using ultrapure deionized water (Milli-Q grade), which exhibited a resistivity higher than 18 MΩ·cm and a total organic content below 6 ppm. This water was produced using the AquaMAX-Ultra 370 Series multicartridge purification system from Young Lin Instrument Co., Ltd. (Gyeonggi-do, Republic of South Korea).

Dispersion Preparation

The dispersions were prepared by weighing the components into vials to determine the composition of the mixtures obtained in terms of weight fraction.[29,30] The components were added sequentially: initially, oleic acid was poured into the vial, followed by the required amount of APG. Finally, Milli-Q water was added to obtain mixtures

https://doi.org/10.1021/acssuschemeng.5c13845
ACS Sustainable Chem. Eng. XXXX, XXX, XXX−XXX

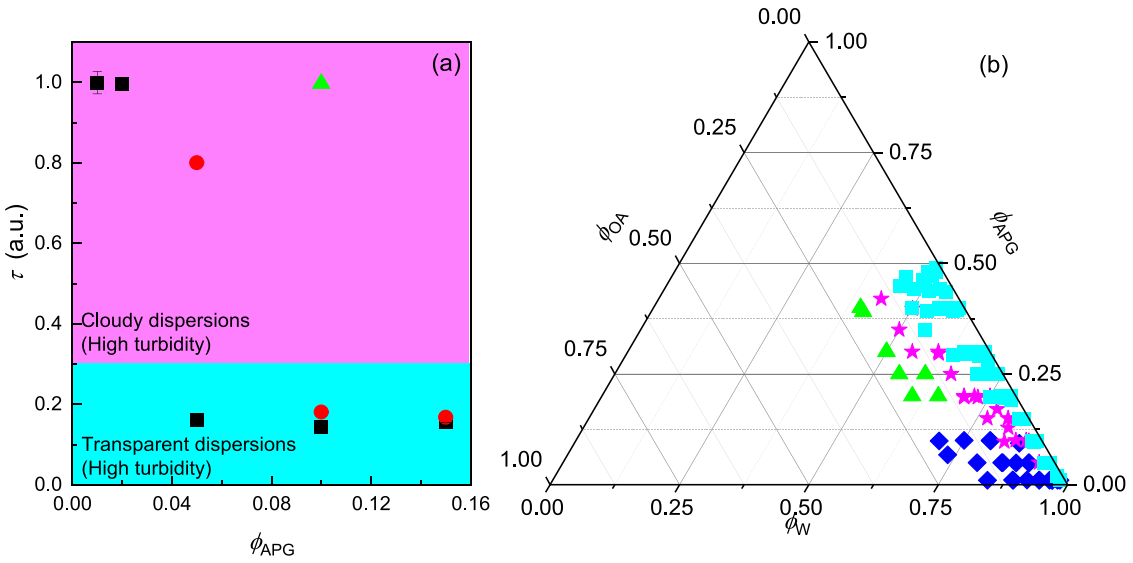


Figure 1. (a) Dependence of the turbidity of selected liquid dispersions on the weight fraction of APG for dispersions with fixed oleic acid weight fractions. The symbols correspond to experimental data: (■) ϕ_{OA} = 0.01, (●) ϕ_{OA} = 0.02 and (▲) ϕ_{OA} = 0.05. Each point represents the average of ten measurements, with deviations smaller than the symbol size. Notice that only the turbidity of single phase liquid-like dispersions. (b) Pseudoternary phase diagram (the whole diagram and a zoom of the studied region are shown) representing a cut of the whole phase diagram obtained at 25 °C for the water/oleic acid/APG system. The different natures of the mixtures obtained are evidenced with different symbols: transparent dispersions (light blue square), cloudy dispersions (pink star), high viscosity dispersions (▲), and phase-separated mixtures (blue diamond solid). Notice that axes represent the weight fraction of the components.

with the desired composition. The samples were then homogenized overnight using a magnetic stirrer at 1200 rpm. All experiments were performed at a controlled temperature of 25.0 ± 0.1 °C. When EOCs such as thymol or carvacrol were incorporated into in the dispersions, they were added prior to emulsification, immediately after the oleic acid to ensure their proper dispersion within the oil phase. To minimize evaporative losses associated with the intrinsic volatility of EOCs, all additions were performed at room temperature (well below the boiling points of both compounds). The oleic acid−EOC mixture was immediately dispersed into the aqueous APG solution, reducing the time during which the essential oil compounds were exposed to air. These precautions ensured that the nominal EOC loading was preserved during sample preparation.

Construction of the Phase Diagram

The phase behavior of the system was mapped by preparing a series of independent mixtures in which the relative proportions of water, alkyl polyglucoside, and oleic acid were systematically varied. After homogenization, each formulation was equilibrated at 25 °C for 24 h and visually examined to determine whether it formed a transparent single-phase dispersion, a turbid dispersion, a phase-separated system, or a highly viscous/structured mixture. This visual categorization was then used to assign each composition to the corresponding region of the pseudoternary diagram. The physical stability of the formulations was evaluated through periodic visual inspection, with most samples showing no evidence of turbidity, creaming, phase separation, or altered flow behavior for periods longer than six months. This represents an improvement over the stability reported previously for systems incorporating soybean lecithin as a cosurfactant.[30] Samples were stored at 25 °C and examined weekly. Throughout this evaluation, the stable formulations remained unchanged, showing no detectable signs of destabilization.

Experimental Techniques

The average apparent size of the oil nanodroplets dispersed in water was determined using dynamic light scattering (DLS), which provide information on the size in terms of the apparent hydrodynamic diameter, d_h^{app}. These measurements were performed using a Zetasizer Nano ZS (Malvern Instruments Ltd., Malvern, UK) that is equipped with a He−Ne laser (wavelength 632 nm) and operates in a quasi-backscattering configuration at a scattering angle of 173°. Before measurements, the samples were filtered through a 0.45 μm pore size inert filter (Fisher Scientific, Hampton, NH, USA) and placed in an optical quartz cuvette (Hellma GmbH and Co. KG, Müllheim, Germany). Additional details on the DLS experiments can be found in previous publications.[30,57]

The overall charge of the complexes was evaluated in terms of their zeta potential (ζ) obtained from electrophoretic mobility measurements performed Laser Doppler Velocimetry using a Zetasizer Nano ZS instrument (Malvern Instruments Ltd., Malvern, UK).

Conductivity measurements of the single-phase dispersions were conducted using a Methrom 856 conductimeter (Methrom AG, Herisau, Switzerland) with a 5-ring platinum conductivity cell (Methrom AG, Herisau, Switzerland). For each dispersion, ten replicate measurements were conducted, resulting in conductivity values with relative standard deviations consistently below 5%.

The pH of the low viscosity single-phase dispersions was measured by the means of a pH-meter (model CG842, Schott GmbH, Columbus, OH, USA) fitted with an electrode Blueline 18 pH (SI Analitycs, Mainz Germany).

The turbidity (τ) of aqueous dispersions was determined from absorbance measurements using the relation $\tau = 1 - 10^{-A}$, where A corresponds to the recorded absorbance. Measurements were carried out at 450 nm with a Jasco V730 spectrophotometer (Jasco Inc., Tokyo, Japan). This wavelength was selected to minimize contributions from the intrinsic absorption features of the individual components.

Fluorescence spectroscopy was employed to study the solubilization of essential oil compounds in oleic acid nanodroplets using an FP-6500 fluorescence spectrophotometer (Jasco Inc., Easton, USA). A fixed excitation wavelength of 280 nm was chosen based on previous studies indicating that this wavelength offers optimal excitation efficiency for essential oil compounds, such as thymol and carvacrol.[58]

RESULTS AND DISCUSSION

Determination of the Pseudoternary Phase Diagram of the Water/Oleic Acid/APG System

The initial step in investigating multicomponent systems, such as the one considered here, involves establishing the

https://doi.org/10.1021/acssuschemeng.5c13845
ACS Sustainable Chem. Eng. XXXX, XXX, XXX−XXX

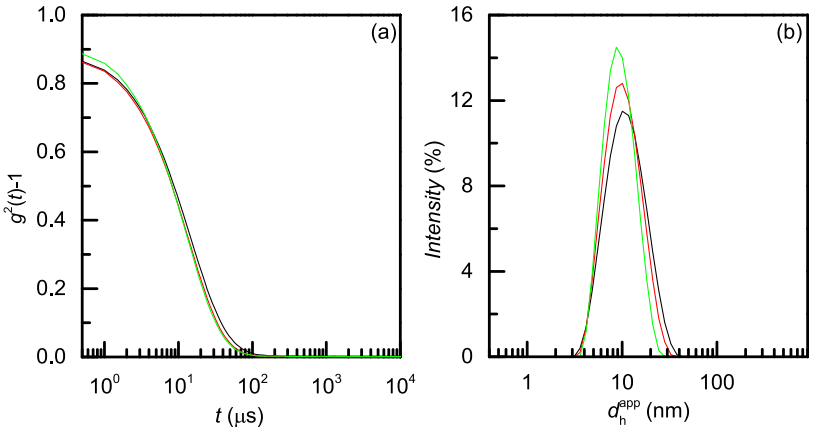


Figure 2. Dynamic light scattering (DLS) analysis of nanodroplet dispersions containing a fixed oleic acid weight fraction of 0.01 and different weight fractions of APG and water. (a) Intensity autocorrelation functions, and (b) intensity-apparent hydrodynamic diameter distributions derived from the analysis of the autocorrelation functions. In both panels, the different curves represent dispersions with different APG weight fractions: (Green dash) ϕ_{APG} = 0.20 (red dash) ϕ_{APG} = 0.30 and (——) ϕ_{APG} = 0.40.

pseudoternary phase diagram. This process requires preparing dispersions where the weight fraction of water, oleic acid, and APG are varied while maintaining a constant pressure (1 atm) and temperature (25 °C). By mapping out this phase diagram, it is possible to distinguish the specific compositional regions in which mixtures lead to stable dispersions (single phase) and in which mixtures phase separate. Therefore, this diagram facilitates an understanding of the type of dispersions formed when the proportions of the different components are adjusted, which is crucial for characterizing the stability region of the system. A visual inspection has been carried out to determine the type of system present for each composition, classifying it into four types: (i) clear dispersions of nanodroplets in water with liquid-like character characterized by low values of turbidity (see Figure 1a); (ii) cloudy dispersions, that could be either emulsions or nanoemulsions, and are characterized by high values of turbidity (see Figure 1a); (iii) high viscosity mixtures; and (iv) systems that exhibit phase separation. Consequently, the area where transparent dispersions are formed, which is the primary focus of this study, is surrounded by regions of cloudy dispersions or phase-separated ones. The pseudoternary phase diagram for the water/oleic acid/APG system under investigation is presented in Figure 1b. This phase diagram represents the concentrations in terms of the weight fraction of the different components ϕ_i, with i being W for water, OA for oleic acid, and APG for alkylpolyglucoside.

The phase diagram reveals that transparent nanodroplet dispersions can be formed within specific weight fraction ranges of oleic acid and APG in the dispersion, specifically 0−0.10 and 0.05−0.49, respectively. It should be noted that the composition of the mixtures were selected to ensure that water was the main component of the mixtures. The phase diagram shows that as the oleic acid fraction increases there is a narrowing of the region in which transparent nanodroplet dispersions can be formed. These transparent systems exhibit several features commonly associated with microemulsions, such as low viscosity and nanometric droplet size, yet, in the absence of thermodynamic evidence, they are more appropriately described as transparent nanodroplet dispersions. This phenomenon can be explained by considering the role of the surfactant in stabilizing the oil droplets. The surfactant is responsible for stabilizing and preventing the droplets from coalescing and phase separating due to its adsorption at the interface between the oil droplets and the water continuous phase. Consequently, to achieve an optimal coating of the droplets, it is essential to increase the surfactant concentration in conjunction with the oleic acid concentration. As the oil weight fraction exceeds the boundaries of the region where transparent dispersions are formed, the system undergoes notable changes. This may be explained by considering that the boundaries of the transparent nanodroplet region (see Figure 1) delineate the compositions yielding stable transparent dispersions of droplets with small sizes (10−15 nm droplets—see discussion of the DLS data in the following section—, >6 months stability). However, the absence of true thermodynamic and/or structural proofs about makes it difficult to identify the true nature of such dispersions. Compositions approaching the limits of the transparent nanodroplet region as a result of the increase in oleic acid content exhibit droplet growth through coalescence and Ostwald ripening, transitioning to turbid dispersions characterized by the presence of droplets with larger average diameters. This transition demonstrates the intricate equilibrium between composition and stability, highlighting the need for precise control over component ratios to maintain the desired single-phase character of the dispersion. A further increase in the oil concentration, while maintaining the APG weight fraction above 0.15, resulted in the formation of highly viscous dispersions that no longer flowed under gravity. This behavior is consistent with a high-volume fraction of oleic acid droplets approaching a percolated, densely packed state, which markedly increases the apparent viscosity of the system. A comprehensive rheological characterization of these concentrated regions, including flow and viscoelastic measurements, lay beyond the scope of the present study. Conversely, for lower values of ϕ_{APG}, coalescence, and Ostwald ripening result in phase separation. The emergence of phase separation at the lowest values of the weight fraction of APG indicates that nanodroplets can only be dispersed in the aqueous phase to give stable dispersions when the surfactant concentration is sufficiently high to guarantee the formation of a stable shell that can prevent phase separation events. Compared with earlier formulations, the present system achieves full stabilization using APG alone, owing to the costabilizing contribution of oleic-acid molecules. This contrasts with

https://doi.org/10.1021/acssuschemeng.5c13845
ACS Sustainable Chem. Eng. XXXX, XXX, XXX−XXX

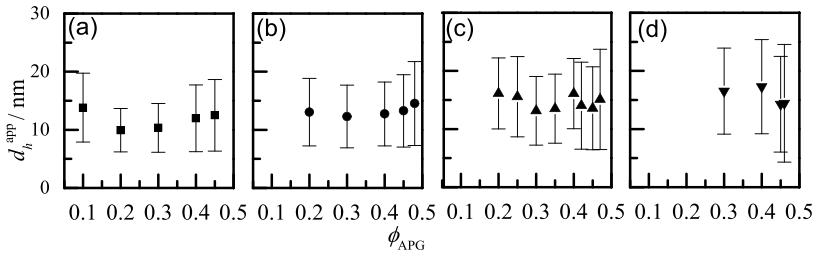


Figure 3. Dependence of the mean apparent hydrodynamic diameter obtained from DLS experiments (symbol) and full width at half-maximum of the apparent hydrodynamic diameter distribution (bars) on the weight fraction of APG in the dispersion for 4 series of samples corresponding to different oleic acid weight fractions. (a) ϕ_{OA} = 0.01, (b) ϕ_{OA} = 0.025, (c) ϕ_{OA} = 0.05, and (d) ϕ_{OA} = 0.075. Note that the bars should not be interpreted as error bars. Instead, they represent the full width at half-maximum (fwhm) of the apparent hydrodynamic diameter in the intensity-weighted distribution.

previous studies that required auxiliary cosurfactants to obtain comparable or enhanced stability, while also simplifying the overall formulation.[29−31] Achieving stable nanodroplets using only APG and oleic acid not only simplifies the system but also reduces the environmental impact associated with solvent production, handling, and disposal. This cosurfactant-free strategy lowers the overall chemical footprint and strengthens the sustainability profile of the formulation, in accordance with green-chemistry principles.

Assessing the Size of the Nanodroplets

Dynamic light scattering (DLS) measurements were employed to estimate the size of the nanodroplets dispersed in the aqueous phase, expressed in terms of their apparent hydrodynamic diameter. This requires analysis of the experimental intensity autocorrelation functions obtained for each dispersion. It should be noted that DLS experiments can only be performed for transparent nonabsorbing solutions with relatively low viscosity; consequently, high viscosity dispersions, cloudy dispersions, and phase-separated samples were excluded from the study. Figure 2 presents a set of intensity autocorrelation functions along with the corresponding intensity distributions derived from their analysis using the CONTIN software. Considering that dispersions studied by DLS contain a relatively small volume fraction of scatterers and low turbidity (see Figure 1a), it can be assumed that single-scattering conditions are guaranteed. Moreover, the use of quasi-backscattering detection during the experiments minimizes the possible contribution of multiple scattering effects.

The intensity autocorrelation functions depicted in Figure 2a reveal that the dynamics of the nanodroplets exhibit a monomodal character that was consistently observed across all compositions examined, confirming negligible interdroplet interactions or scattering artifacts. This trend is further corroborated by Figure 2b, which illustrates the intensity distributions derived from the analysis of the autocorrelation data and provides a clear illustration of the aforementioned behavior. The results indicate the presence of a single population on the apparent hydrodynamic diameter distribution. This observation is consistent with the monomodal character exhibited by the intensity autocorrelation functions. It is important to note that the observed shift in intensity distributions is not significant when considering the scale of the apparent hydrodynamic diameter obtained for the droplets, which is on the order of a few nanometers. Therefore, it can be assumed that the mean droplet size remains essentially unchanged as the surfactant concentration increases at fixed oleic acid concentration. This is shown in Figure 3 where the dependence of the apparent hydrodynamic diameter of the nanodroplets on the APG weight fraction is plotted for dispersions with different oil concentrations. The mean apparent hydrodynamic diameter was determined through the application of the Stokes−Einstein equation, which establishes a relationship between the average apparent diffusion coefficient (D_{app}) and the apparent hydrodynamic diameter (d_h^{app}) as $d_h^{app} = k_B T/3\pi\eta D_{app}$. In this relationship, k_B is the Boltzmann constant, T is the absolute temperature, and η denotes the shear viscosity of the continuous medium.

The data indicate that the nanodroplets consistently exhibit a mean hydrodynamic diameter between 10 and 15 nm, independent of the concentrations of APG or oleic acid. When compared with the hydrodynamic diameter of APG micelles (6.4 ± 0.5)nm, it becomes evident that the droplets behave essentially as APG micelles swollen by the oil incorporation. This supports the interpretation that the system consists of a dispersion of noninteracting swollen micelles, in which the oil distributes uniformly among a growing number of droplets as the APG concentration increases ($N \propto$ APG concentration). The presence of monomodal correlation functions further confirms the absence of significant interparticle interactions or multiple scattering phenomena. Overall, the findings show that APG alone provides sufficient stabilization for the nanodroplets, eliminating the need for additional stabilizing agents. The very small changes in average droplet size with increasing APG concentration (Figure 3) suggest the formation of a robust interfacial layer that effectively suppresses coalescence and limits Ostwald ripening.

A closer look at the dependence of the droplet size on oleic acid concentration reveals an increase in the mean droplet size (symbols in Figure 3) and polydispersity (represented as the full width at half-maximum (FWHM) of the apparent hydrodynamic diameter in the intensity-weighted distribution reported as bars in Figure 3) as the oleic acid concentration rises. This observation is related to the incorporation of a higher amount of oleic acid into the swollen micelles. On the other hand, the nonvariation of mean droplet size with increasing APG weight fraction is reminiscent of the behavior of a micellar system with nonstrong interactions.

The nanodroplets characterized in this work exhibit mean hydrodynamic diameters in the 10−15 nm range. Direct imaging of the nanodroplets (e.g., by TEM or cryo-TEM) was not performed in this study, as structures of this size composed of soft, low-contrast organic materials typically require specialized cryogenic preparation and phase-contrast enhancement to be reliably visualized;[59−61] however, the structural interpretation presented here consistently indicate the formation of swollen APG-stabilized oleic-acid nano-

https://doi.org/10.1021/acssuschemeng.5c13845
ACS Sustainable Chem. Eng. XXXX, XXX, XXX−XXX

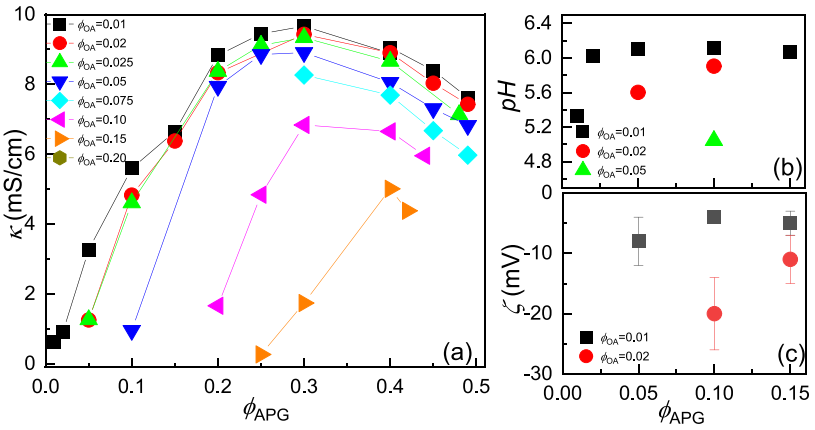


Figure 4. (a) Dependence of the ionic conductivity on the weight fraction of APG for dispersions with fixed oleic acid weight fractions. (b) Dependence of the pH on the weight fraction of APG for dispersions with fixed oleic acid weight fractions. (c) Dependence of the zeta potential (ζ) on the weight fraction of APG for dispersions with fixed oleic acid weight fractions. The symbols correspond to experimental data, while the lines serve only as visual guides. Each point represents the average of ten measurements, with deviations smaller than the symbol size in all cases except for the zeta potential data.

droplets with a hydrophobic core surrounded by an interfacial region.[62,63]

Ionic Conductimetry and pH of the Dispersions

Ionic conductivity (κ) measurements in dispersions provide valuable insights into the distribution of various species with ionic character within the system. This property is particularly susceptible to changes in the weight fraction of the dispersed phase and its composition, particularly when specific species within the oil phase exhibit a marked preference for positioning themselves at the droplet interfaces. In the system under examination, the conductivity of the dispersion can be attributed mainly to the presence of oleic acid, both within the droplet and at the droplet/continuous phase interface. Figure 4a provides a visual representation of the relationship between ionic conductivity and the weight fraction of APG for dispersions with fixed oil weight fractions.

The results show that, regardless of the weight fraction of oleic acid, an increase in the APG weight fraction initially enhances the conductivity of the dispersion, until it reaches a maximum value before decreasing as the APG content continues to rise. First, the observed ionic conductivity in dispersions stabilized by a neutral surfactant, such as APG, can only be explained by the incorporation of a portion of the oleic acid molecules into the surfactant layer adsorbed at the nanodroplet/continuous phase interface. These oleic acid molecules, due to their dissociation, contribute to the ionic conductivity of the nanodroplets.

Focusing on the effect of the surfactant weight fraction on conductivity, the initial increase in conductivity with rising APG content suggests that higher APG concentrations lead to an increase in the number of charge carriers in the system, i.e., number of charged droplets, thereby increasing conductivity. This interpretation is consistent with the absence of significant changes in the apparent hydrodynamic diameter as the APG weight fraction increases at a fixed oleic acid content, indicating that the system accommodates more charge carriers without altering droplet size. On the other hand, the observed decrease in conductivity at higher APG weight fractions implies the appearance of an antagonist effect which counteracts the effect of the increase in the number of carriers. Thus, once the APG content in the dispersions overcomes a threshold value, the resulting increase in dispersion viscosity counteracts the conductivity gains associated with the formation of additional charge carriers. This viscosity resistance to ionic movement ultimately reduces the overall conductivity. The pH trends appear to contradict the conductivity measurements of the dispersions (see Figure 4b). As the APG content increases at a fixed oleic acid weight fraction, both conductivity and pH increase. The increase in pH suggests a reduction in the number of dissociated oleic acid molecules in contact with the aqueous phase. This can be explained by considering that higher APG concentrations increase the number of nanodroplets as was claimed based on the conductivity results. This leads to the sequestering of a larger fraction of oleic acid molecules within the low-polarity core of the nanodroplets where dissociation is inhibited. Consequently, the bulk aqueous concentration of H^+ decreases, causing the pH to increase. It is worth noting that this reduction of the concentration of H^+ in the aqueous medium and of the net charge per droplet which are associated with the pH reduction are counteracted with the increases in the total number of charged droplets, resulting in enhanced conductivity.

Figure 4 also illustrates the effect of varying the oleic acid weight fraction (at constant APG content) on conductivity and pH. As the oleic acid content increases, both the ionic conductivity of the nanodroplet dispersions and their pH drops. This behavior is due to droplet swelling as higher oleic acid concentrations result in larger nanodroplets, exposing more oleic acid molecules to the aqueous phase. This increased exposure raises the number of dissociated carboxylate groups and therefore the H^+ concentration, which lowers the pH. However, despite the higher density of ionic groups, the increase in the number of droplets reduces their mobility, ultimately diminishing the overall ionic conductivity. Electrophoretic mobility measurements on dilute, optically transparent dispersions (ϕ_{OA} = 0.01−0.02, ϕ_{APG} = 0.05−0.15) were carried out to determine the effective charge of the nanodroplets through evaluation of the zeta potential (ζ). The measured zeta potentials ranged from approximately −10 mV (at the highest APG weight fractions or the lowest OA weights fractions) to −25 mV (at the lowest APG weight fractions or the highest OA weight fractions), as detailed in Figure 4c.

https://doi.org/10.1021/acssuschemeng.5c13845
ACS Sustainable Chem. Eng. XXXX, XXX, XXX−XXX

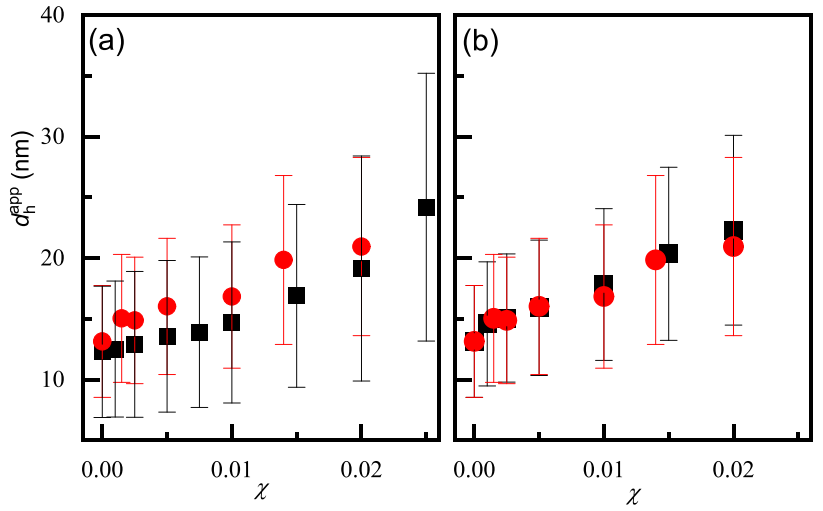


Figure 5. (a) Dependence of the mean apparent hydrodynamic diameter obtained from DLS experiments (symbol) and full width at half-maximum of the apparent hydrodynamic diameter distribution (bars) for oil nanodroplets on the weight fraction of carvacrol solubilized for dispersions with a weight fraction of oleic acid of 0.05 and two different APG weight fractions of 0.25 (■) and 0.30 (●). (b) Dependence of the mean apparent hydrodynamic diameter obtained from DLS experiments (symbol) and full width at half-maximum of the apparent hydrodynamic diameter distribution (bars) on the weight fraction of thymol (■) and carvacrol (●) solubilized for dispersions with weight fractions of oleic acid and APG of 0.05 and 0.30, respectively. Note that the bars should not be interpreted as error bars. Instead, they represent the full width at half-maximum (fwhm) of the apparent hydrodynamic diameter in the intensity-weighted distribution.

These measurements further confirmed the pH-dependent negative charging arising from oleate dissociation. Specifically, the results show that decreasing ϕ_{OA} leads to higher (i.e., less negative) zeta potential values at a fixed surfactant concentration, consistent with a reduced number of dissociated oleate groups exposed to the aqueous phase, as previously inferred from the pH data. Moreover, increasing the APG weight fraction at a constant oleic acid content also results in higher zeta potentials, again indicating less negative values. This trend aligns with the observed pH increase and the corresponding decrease in the amount of dissociated carboxylate groups exposed to the aqueous phase. It is worth noting that, these low values of zeta potential found in our systems contrast sharply with the high charge densities typically required (>±30 mV, often >±40 mV) for purely electrostatically stabilized colloidal systems, where DLVO theory predicts that strong double-layer repulsion is essential to overcome attractive van der Waals forces between particles.[64] In such ionic systems, stability fails rapidly below $\zeta \approx \pm 30$ mV due to an insufficient energy barrier for aggregation, particularly in low-ionic-strength media where Debye screening is minimal.[65] Here, the modest electrostatic contribution from oleate dissociation acts primarily as a secondary stabilizer that complements the dominant steric barrier provided by the densely grafted APG chains at the oil−water interface. The extended hydrophilic headgroups of caprylyl/capryl glucosides create an entropic repulsion that effectively prevents close particle encounters even at low ζ, explaining the observed >6-month stability of transparent dispersions despite zeta potentials far below the electrostatic threshold.[66] This hybrid stabilization mechanism, low-magnitude charging plus nonionic steric hindrance, is characteristic of "practical" nanoemulsions and swollen micelles used in cosmetics and food formulations, where high ionic strength or extreme pH would otherwise screen o or reverse the charge.[67,68]

Effect of the Dispersion of Essential Oil Components within the Nanodroplets

Essential oil components are multifunctional molecules, yet their poor water solubility and chemical lability make encapsulation necessary to preserve their activity. In the case of thymol and carvacrol, their moderate volatility adds an additional challenge. Incorporating these compounds into fatty nanodroplets not only enhances their solubility but also mitigates evaporative losses, a limitation in essential oil formulations. This work studies the solubilization of two isomeric essential oil compounds, namely thymol and carvacrol. The compositions selected for studying the solubilization of thymol and carvacrol lie approximately at the center of the transparent-dispersion region identified in the pseudoternary phase diagram (Figure 1). This region corresponds to formulations that consistently yield stable, low-viscosity nanodroplets suitable for DLS, conductivity, and fluorescence measurements. Choosing compositions well within this stability window minimizes boundary effects, such as droplet growth, turbidity, or gelation, that occur near the limits of the one-phase region. The same rationale applies to all experiments involving essential oil compound incorporation, ensuring that the observed changes arise from EOC solubilization rather than from intrinsic instabilities of the underlying dispersion. It is important to note that the optimal composition for nanodroplet formation is not expected to be significantly influenced by the identity of the encapsulated essential oil compound. Although thymol is a solid at room temperature and carvacrol is a liquid, both molecules are structural isomers with closely comparable hydrophobicity and molecular size. These similarities should favor a similar partitioning behavior within the oleic-acid core once solubilized.

As first test to evaluate the dispersion of the essential oil compounds within the nanodroplets, DLS measurements were performed, which provide information on changes in the apparent size of the nanodroplets with the inclusion of

https://doi.org/10.1021/acssuschemeng.5c13845
ACS Sustainable Chem. Eng. XXXX, XXX, XXX−XXX

essential oils. Figure 5 shows the dependence of the mean apparent hydrodynamic diameter of the nanodroplets on the weight fraction of the essential oil compound solubilized (χ).

The incorporation of essential oil compounds (EOCs) into the oil nanodroplets increases the mean apparent hydrodynamic diameter because they expand the volume of the hydrophobic core. As a result, the ratio of surfactant to dispersed oil phase decreases, meaning that a higher surfactant concentration would be required to maintain a constant droplet size. When EOCs are added at fixed surfactant and oleic acid weight fractions, the droplets grow because solubilization effectively shifts the formulation toward the boundary regions of the phase diagram, reducing the effective surfactant-to-oil ratio. This effect becomes critical when thymol or carvacrol exceed their threshold loadings (~0.02), at which point destabilization is promoted.

In the absence of EOCs, the dispersed phase consists mainly of oleic acid, and APG molecules form a mixed interfacial layer with adsorbed oleic acid, providing steric and electrostatic stabilization. Upon incorporation of thymol or carvacrol, these compounds behave as additional oil-like components within the droplet core, increasing the total dispersed-phase volume while the amount of APG available for interfacial coverage remains constant. Consequently, the effective surfactant-to-oil ratio decreases.[69] At low EOC loadings, APG is still sufficient to stabilize the enlarged droplets, resulting in only moderate size increases. However, when the EOC fraction surpasses ~0.02, the interfacial layer can no longer maintain a compact, defect-free film. The reduced surfactant coverage facilitates droplet growth through coalescence and Ostwald ripening, leading to a pronounced increase in droplet size and, ultimately, turbidity and phase separation as the formulation approaches the edge of the transparent region.[67,69] This behavior highlights the sensitivity of the formulation window and provides guidance for maintaining stability during scale-up.

It is worth noting that neither the type of solubilized essential oil compound nor the composition of the dispersion used for the solubilization of the essential oil compounds results in noticeable differences on the solubilization process. The effect of the former parameter can be rationalized by considering that we are comparing the solubilization of two isomers and therefore, it cannot be expected a significant change in their molecular size, which leads to a similar influence in the droplet sizes upon solubilization. In relation to the role of the composition of the dispersion used for EOC solubilization, the absence of influence of this parameter can be considered a result of the almost negligible influence of the dispersion composition on the nanodroplet size (see Figure 4). It is worth noting that although the encapsulation efficiency was not explicitly quantified, the absence of visible phase separation, such as solid thymol crystals or carvacrol macrodroplets, and the lack of secondary size populations in the DLS distributions indicate that both compounds are fully incorporated into the oleic acid core under the conditions investigated

Ionic conductivity measurements were performed to deepen understanding of the incorporation of the essential compounds into the oleic acid nanodroplets. Figure 6 shows the dependence of the ionic conductivity on the weight fraction of essential oil compound solubilized into nanodroplets of dispersions with a fixed composition.

The ionic conductivity decreases as the amount of essential oil compounds in the oil phase increases. This behavior can be

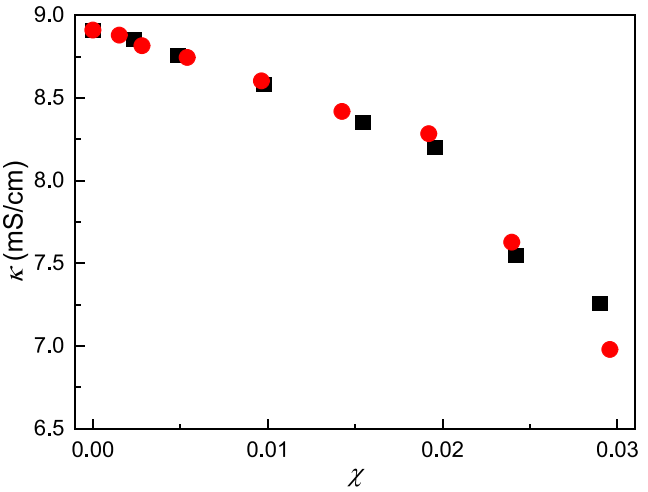


Figure 6. Dependence of the ionic conductivity of the dispersions on the weight fraction of thymol (■) and carvacrol (●) solubilized for dispersions with weight fractions of oleic acid and APG of 0.05 and 0.30, respectively. The results are the average value of ten measurements, and their average deviation is smaller than the point dimensions.

partially attributed to the hydrotropic properties of EOCs, which are known to enhance the solubility of hydrophobic molecules in aqueous systems by modifying the interfacial environment. In our system, the addition of EOCs leads to a reduction in ionic conductivity (Figure 6), suggesting a shift in the interfacial composition, potentially due to the displacement of oleic acid molecules from the interface into the droplet core. Consequently, as the concentration of the essential oil compound increases, it displaces oleic acid from the interface to the oil phase core, thereby reducing the number of oleic acid molecules with dissociated carboxylate groups that are exposed to the aqueous phase. This reduction in the number of exposed ions results in a decrease in average conductivity due to a lower concentration of free ions. The concomitant decrease in interfacial oleate density implies a weakening of the electrostatic contribution to nanodroplet stabilization, which, combined with the EOC-induced swelling of the hydrophobic core, further accentuates the drop in the effective surfactant-to-oil ratio and promotes destabilization at high EOC loadings.[69]

These findings emphasize that nanodroplet stabilization is not solely dependent on the formation of a surfactant film at the droplet/aqueous phase interface; the adsorption of oleic acid molecules from the oil phase to this interface also plays a significant role. Consequently, the oleic acid content within the dispersion emerges as a critical factor in ensuring the stability of nanodroplet dispersions in agreement with previous results on emulsion-like systems involving oleic acid.[29−31,70]

Unraveling the Molecular Mechanisms of Dispersion of Essential Oil Compound within Nanodroplets

Fluorescence emission spectroscopy, it is sensitive to the chemical environment surrounding fluorescent molecules[71] and it was employed in this study to investigate the chemical environment and the aggregation behavior of essential oil molecules. Therefore, it is used to provide insights into the solubilization mechanism of the essential oil compounds within the nanodroplets, following for this purpose a procedure adapted from our previous work.[30] Here, the changes in the fluorescence properties of the essential compounds resulting from its solubilization within oleic acid nanodroplets stabilized

https://doi.org/10.1021/acssuschemeng.5c13845
ACS Sustainable Chem. Eng. XXXX, XXX, XXX−XXX

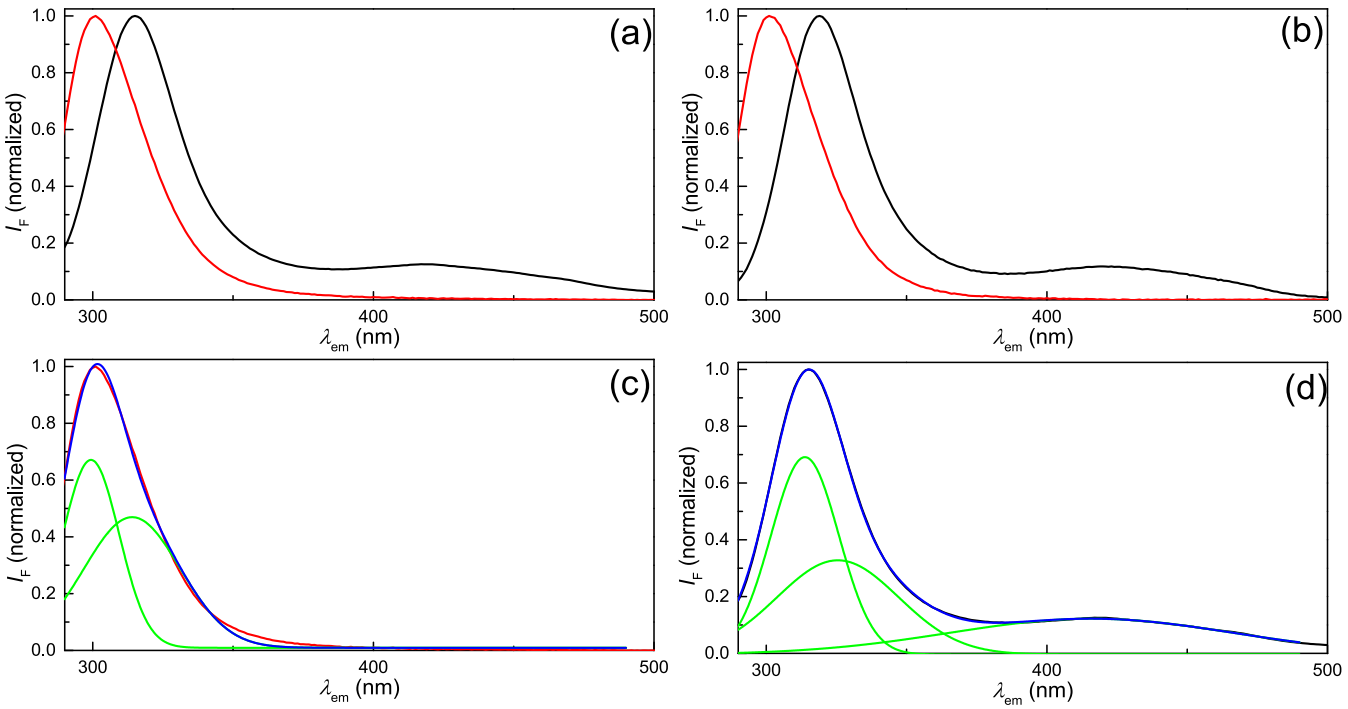


Figure 7. Normalized fluorescence emission spectra (excitation wavelength 280 nm). (a) Fluorescence spectra corresponding to a solution of carvacrol in oleic acid with a weight fraction of the EOC of 0.02 (——) and to the EOC entrapped in oleic acid nanodroplets (weight fractions of oil phase and APG of 0.05 and 0.30 respectively, with a carvacrol weight fraction of 0.02) (red dash). (b) Normalized fluorescence spectra corresponding to a solution of thymol in oleic acid with a weight fraction of the EOC of 0.02 (——) and to the essential oil compound entrapped in oleic acid nanodroplets (weight fractions of oil phase and APG of 0.05 and 0.30 respectively, with a thymol weight fraction of 0.02) (red dash). (c) Normalized spectra (red dash) and separated (blue dash) spectra, together with the different Gaussian bands obtained from the separation procedure (green dash), for a solution of carvacrol in oleic acid with a weight fraction of the EOC of 0.02. (d) Normalized spectra (red dash) and separated (blue dash) spectra, together with the different Gaussian bands obtained from the separation procedure (green dash), for a nanodroplet dispersion containing carvacrol (weight fractions of oil phase and APG of 0.05 and 0.30, respectively, with a carvacrol weight fraction of 0.02).

by APG are explored. Figure 7 presents the fluorescence spectra, plotted as fluorescence intensity (I_F) versus emission wavelength (λ_{em}), for the essential oil compounds in two different environments: in solution within oleic acid and incorporated in oleic acid nanodroplets stabilized by APG. Figure 7a,b highlight the differences in the fluorescence emission spectra for thymol and carvacrol depending on its solubilization environment. Notably, the encapsulation process induces two main changes in the fluorescence emission profile. First, the emission peak shifts to different wavelengths, indicating a distinct chemical environment. Second, the band structure differs, with an additional band appearing when the essential oil is encapsulated in the nanodroplets compared to when it is simply dissolved in oleic acid. To clarify these differences, the spectra were separated into Gaussian bands (deconvolution procedure), providing a more detailed representation of the transitions contributing to the fluorescence spectrum in each case. The deconvolution procedure is clearly illustrated in Figure 7c,d, where carvacrol is used as a model compound to exemplify the observed behavior (a comparable response was also found for thymol, this is expected due to the similarities found in the spectrum profiles for carvacrol and thymol reported in Figure 7a,b, respectively). Figure 7c shows the experimental spectrum of a carvacrol solution in oleic acid, together with the individual bands obtained from the deconvolution of the experimental spectrum and the corresponding calculated spectrum. Analogous results are presented in Figure 7d for an oleic acid nanodroplet dispersion stabilized by APG, with carvacrol incorporated into the inner core of the nanodroplets. The distinct band profiles resulting from the spectral deconvolution highlight the structural changes in fluorescence properties induced by the interaction of the essential oils with the nanodroplet environment.

The emission spectrum corresponding to a carvacrol solution in oleic acid (see Figure 7c) presents a band with its maximum observed around 300 nm. However, a closer examination of the spectrum suggests the presence of distinct peaks with Gaussian profiles, which can be clearly resolved by the deconvolution procedure. This analysis (see Figure 7c) shows that carvacrol dissolved in oleic acid exhibits two well-defined spectral bands centered at 299 and 314 nm, respectively. The presence of these two bands is consistent with the formation of carvacrol clusters, as reported in the literature for similar aromatic alcohols.[72] Therefore, one band is likely associated with isolated carvacrol molecules, while the other corresponds to clusters of multiple thymol molecules. Compared to isolated carvacrol molecules, the interactions within these clusters result in energy dissipation, which leads to a red shift in the central wavelength of the emission spectrum associated with the clusters. This red shift highlights the impact of molecular aggregation on the photophysical properties of carvacrol in the oleic acid medium.[31] It is worth noting that the behavior of thymol solutions in oleic acid is similar to that discussed for the carvacrol. The same applied when the solubilization in nanodroplet dispersions is considered.

The solubilization process of the essential oil compounds in the oily core of nanodroplets induces changes in the

https://doi.org/10.1021/acssuschemeng.5c13845
ACS Sustainable Chem. Eng. XXXX, XXX, XXX−XXX

fluorescence emission properties of the EOCs in relation to the situation in which the EOC is simply solubilized in oleic acid (see Figure 7d). Specifically, the emission maximum centered for the essential oil compounds dissolved in oleic acid around 300 nm undergoes a bathochromic shift to 315−320 nm (similar shift is observed for thymol), reflecting the altered chemical environment surrounding the EOC molecules as a result of the solubilization within the oil nanodroplets. Additionally, the interpretation of the fluorescence emission spectrum corresponding to the essential oil solubilized into the oily core of the oleic acid nanodroplets is less straightforward, appearing an additional band. This can be attributed to the emergence of new chemical microenvironments created by the solubilization process, which differ from the environment present in the solutions of essential oil compounds in oleic acid. These microenvironments likely arise from interactions between the essential oil compounds and the components of the nanodroplets, influencing the electronic transitions responsible for the observed fluorescence behavior. Thus, the fluorescence emission spectra of the EOCs encapsulated within the oily core of the nanodroplets include three different bands centered around 315, 335, and 420 nm, respectively.

Based on the above analysis, the three different bands observed in the spectra of the dispersions can be attributed to specific solubilization environments of thymol within the nanodroplets: (i) the band centered around 315 nm is attributed to individual essential oil compound molecules solubilized within the nanodroplet interior (Band I); (ii) the band centered around 335 nm is associated with EOC clusters formed within the nanodroplet core (Band II); and (iii) the band centered around 420 nm corresponds to EOC molecules localized near the interfacial region of the nanodroplets (Band III). The origin of Band III is consistent with previous studies reporting that thymol solubilized in microemulsion nanodroplets exhibits an emission band analogous to Band III, which was attributed to thymol molecules residing in a chemical microenvironment characteristic of the interfacial region of microemulsion droplets.[73,74] The assignment of Bands I and II relies on their similarity to those observed for EOC solutions in oleic acid. As previously discussed, two bands appear in oleic-acid solutions of the EOCs, and the Band I and Band II features in the nanodroplet dispersions closely resemble those solution bands, with the only difference being a shift to higher wavelengths. This red shift is consistent with the confinement of thymol within the inner core of the oleic-acid nanodroplets. This comparison also supports the interpretation that the additional band observed in the dispersions (Band III) corresponds to the emission of EOC molecules located in the new chemical microenvironment created by their confinement within the nanodroplet structure. The presence of three distinct microenvironments suggests that EOC release under application conditions may follow a heterogeneous, multistage kinetic profile. Compared to uniform core solubilization, this type of profile combines immediate bioavailability with prolonged activity, potentially extending the duration of antimicrobial activity. Figure 8 presents a comparison of the emission spectra for dispersions with fixed oleic acid (0.05) and APG (0.30) weight fractions, respectively, and varying weight fractions of solubilized thymol.

The analysis of fluorescence spectra of the as a function of the essential oil concentration for dispersions with a fixed composition reveals differences in the intensity of the emission bands. In fact, the emission intensity shows a notable

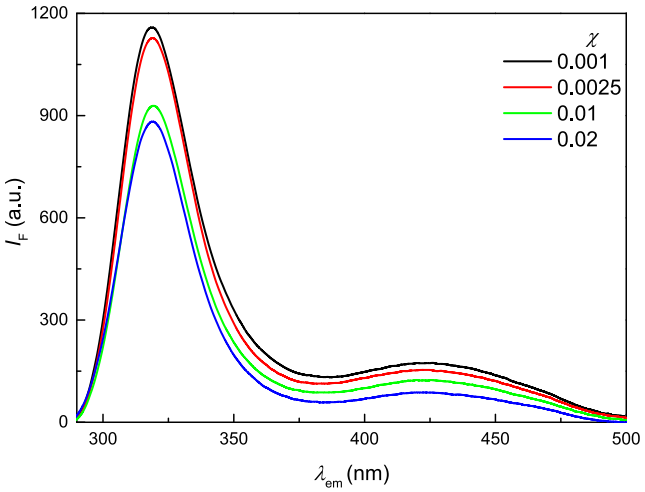


Figure 8. Comparison of fluorescence emission spectra for dispersions with an increasing concentration of thymol dissolved within the oily core of the nanodroplets (dispersion with weight fractions of oil phase and APG of 0.05 and 0.30, respectively). Each curve corresponds to the fluorescence spectra of a dispersion with different weight fraction of carvacrol encapsulated.

dependence on the essential oil compound concentration within the oil phase, with the fluorescence intensity decreasing as the essential oil compound concentration increases. This trend is indicative of a self-quenching effect, which can be attributed to the spatial confinement of essential oil compound molecules incorporated within the inner core of the nanodroplets. At higher concentrations, the limited volume of droplets leads to significant molecular crowding. This proximity promotes intermolecular interactions, resulting in aggregate formation that diminishes fluorescence intensity. The self-quenching effect arising from molecular confinement becomes evident when examining the results in Figure 9. The figure presents the evolution of the integrated emission intensities of the three fluorescence bands as a function of the EOC weight fraction in dispersions of fixed composition. A systematic decrease in band intensity is observed as the amount of solubilized EOC increases. This attenuation of fluorescence is fully consistent with the self-quenching mechanism discussed above, reflecting the reduced intermolecular distances within the confined oil phase.

CONCLUSIONS

This study examines how oleic acid enables the dispersion of essential oil compounds into nanoscale droplets in water and how an alkylpolyglucoside surfactant stabilizes these structures by forming a robust interfacial layer. This simple and scalable formulation strategy provides an efficient route for encapsulating hydrophobic essential oil components. This study demonstrates that achieving stable aqueous nanodroplets for the solubilization of essential oil compounds requires precise control over formulation composition. Oleic acid plays a central role by providing an effective medium for incorporating the bioactives, yet the overall stability of the dispersions is dictated by the maximum oil load that can be accommodated at a given surfactant concentration. Systematic analysis of the oleic acid/APG/EOC interplay reveals subtle but important effects, such as the mild hydrotropic behavior of the essential oil compounds and their influence on interfacial structure, that govern long-term stability. Increasing the essential oil content

https://doi.org/10.1021/acssuschemeng.5c13845
ACS Sustainable Chem. Eng. XXXX, XXX, XXX−XXX

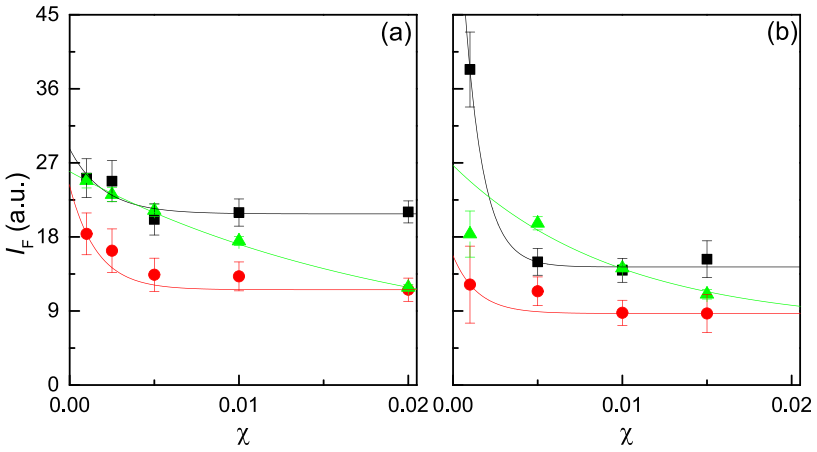


Figure 9. Dependence of fluorescence intensity for the three emission bands for dispersion with weight fractions of oleic acid and APG of 0.05 and 0.30, respectively, solubilizing thymol (a) and carvacrol (b). The symbols correspond to the experimental results and the solid lines are guides for the eyes. In both panel: (■) Band I, (●) Band 2 and (▲) Band III.

enlarges droplet size and enhances susceptibility to destabilization mechanisms, including coalescence and Ostwald ripening, because the added EOCs effectively decrease the surfactant-to-oil ratio at fixed APG and oleic-acid contents, thereby defining an upper limit to the achievable payload. Oleic acid content thus emerges as a key stabilizing factor, whereas excessive incorporation of essential oil compounds, although desirable for functionality, can compromise dispersion integrity. These findings highlight the need for careful compositional optimization to balance high bioactive loading with robust colloidal stability.

Fluorescence spectroscopy revealed that essential oil compounds are not uniformly distributed within the nanodroplets but instead occupy multiple microenvironments, ranging from molecules dissolved in the droplet interior to aggregated domains and species located near the interfacial region. This structural heterogeneity provides important insight into the solubilization pathways and stabilization mechanisms operating within the droplets. Beyond advancing the fundamental understanding of EOC encapsulation, these findings offer practical guidance for designing nanodroplet systems capable of efficiently delivering poorly water-soluble bioactives. The balance between oleic acid, surfactant, and essential oil content emerges as a key determinant of both loading capacity and long-term stability, with direct implications for applications in pharmaceuticals, food preservation, and cosmetics. According to the results, optimal formulations for technological applications are expected to lie near the center of the transparent region, whereas compositions close to the phase-boundary are more prone to turbidity, gelation, or phase separation, which may restrict their practical use. Consequently, the phase diagram provides a straightforward tool for selecting suitable formulations based on application requirements (e.g., dilute sprays: low ϕ_{OA}; viscous creams: higher ϕ_{APG}). Moreover, the use of APG as a biodegradable, biocompatible stabilizer provides a scalable and environmentally responsible alternative to formulations relying on synthetic surfactants or cosolvents.

Finally, while the present work relies on pure model components, translating this platform to industrial scale requires validation with waste-derived oleic acid streams and thymol and carvacrol obtained from plant essential oils. The pseudoternary methodology established here enables rapid assessment (<24 h) of phase behavior changes due to impurities (saturates, oxidation products), guiding feedstock selection. This would further improve the overall sustainability and circularity of the platform. In this context, future work should further assess the long-term stability and biodegradability of these systems to consolidate their potential for sustainable industrial implementation. Moreover, a systematic comparison of the antimicrobial activity of encapsulated versus free EOCs (minimal inhibitory concentration (MIC)/minimal bactericidal concentration (MBC) assays and tests in practical systems) should be also considered as a key direction for future work.

AUTHOR INFORMATION

Corresponding Author

Eduardo Guzmán − *Departamento de Química Física, Facultad de Ciencias Químicas, Universidad Complutense de Madrid, 28040 Madrid, Spain; Instituto Pluridisciplinar, Universidad Complutense de Madrid, Paseo Juan XXIII 1, Ciudad Universitaria, 28040 Madrid, Spain;* orcid.org/0000-0002-4682-2734; Phone: +34 913944107; Email: eduardogs@quim.ucm.es; Fax: +34 913944135

Authors

Laura Fernández-Peña − *Departamento de Química Física, Facultad de Ciencias Químicas, Universidad Complutense de Madrid, 28040 Madrid, Spain;* Present Address: Departamento de Tecnología Química, Energética y Mecánica, Escuela Superior de Ciencias Experimentales y Tecnología, Universidad Rey Juan Carlos (Campus de Móstoles), Avenida del Alcalde de Móstoles, 28933 Móstoles, Spain; orcid.org/0000-0002-8795-8769

Emilie Larguier − *École Nationale Supérieure de Chimie de Lille, Centrale Lille, 59652 Villeneuve D'Ascq, France*

Solange d'Aligny − *École Nationale Supérieure de Chimie de Lille, Centrale Lille, 59652 Villeneuve D'Ascq, France*

Alejandro Toledo-Sánchez − *Departamento de Química Física, Facultad de Ciencias Químicas, Universidad Complutense de Madrid, 28040 Madrid, Spain*

Paula Porawski-González − *Departamento de Química Física, Facultad de Ciencias Químicas, Universidad Complutense de Madrid, 28040 Madrid, Spain*

https://doi.org/10.1021/acssuschemeng.5c13845
ACS Sustainable Chem. Eng. XXXX, XXX, XXX−XXX

Alejandro Lucia − *Grupo de Manejo Integrado y Bioecología de Artrópodos Dulceacuícolas (MIyBAD)—Instituto de Ecología y Desarrollo Sustentable (INEDES, CONICET-UNLu), 6700 Luján, Buenos Aires, Argentina;* orcid.org/0000-0003-3305-5342

Chaïma Amara − *École Nationale Supérieure de Chimie de Paris-ParisTech, Université Paris Sciences et Lettres, 75231 Paris, France*

Francisco Ortega − *Departamento de Química Física, Facultad de Ciencias Químicas, Universidad Complutense de Madrid, 28040 Madrid, Spain; Instituto Pluridisciplinar, Universidad Complutense de Madrid, Paseo Juan XXIII 1, Ciudad Universitaria, 28040 Madrid, Spain*

Ramón G. Rubio − *Departamento de Química Física, Facultad de Ciencias Químicas, Universidad Complutense de Madrid, 28040 Madrid, Spain; Instituto Pluridisciplinar, Universidad Complutense de Madrid, Paseo Juan XXIII 1, Ciudad Universitaria, 28040 Madrid, Spain*

Complete contact information is available at: https://pubs.acs.org/10.1021/acssuschemeng.5c13845

Author Contributions

L.F.-P.: Methodology, Formal analysis, Investigation, Data Curation, Supervision. E.L.: Investigation. S.d'A.: Investigation. A.T.-S.: Investigation. P.P.-G.: Investigation. A.L.: Conceptualization, Investigation, Writing—Review & Editing. C.A.: Investigation. F.O.: Investigation, Resources, Writing—Review & Editing, Project administration, Funding acquisition. R.G.R.: Validation, Resources, Investigation, Writing—Review & Editing, Supervision, Project administration, Funding acquisition. E.G.: Conceptualization, Methodology, Software, Validation, Formal analysis, Resources, Data Curation, Writing—Original Draft, Visualization, Supervision, Project administration, Funding acquisition.

Notes

The authors declare no competing financial interest.

■ ACKNOWLEDGMENTS

This work was supported by the grant PID2023-147156NB-I00, funded by MCIN/AEI/10.13039/501100011033 (Spain). A.L. also acknowledges the financial support by Agencia Nacional de Promoción Científica y Técnica (ANPCyT) under the grant PICT-2021-GRF-TI-00704. The authors express their gratitude to the Unidad de Espectroscopía y Correlación (CAI de Técnicas Químicas) at Universidad Complutense de Madrid for granting access to their facilities. The graphical abstract has been created by using SMART (Servier Medical Art) licensed Creative Commons Attribution 4.0 and Biorender (https://www.biorender.com/).

■ REFERENCES

(1) Guzmán, E.; Lucia, A. Essential Oils and Their Individual Components in Cosmetic Products. *Cosmetics* **2021**, *8*, No. 114.

(2) Lucia, A.; Guzmán, E. Emulsions Containing Essential Oils, Their Components or Volatile Semiochemicals as Promising Tools for Insect Pest and Pathogen Management. *Adv. Colloid Interface Sci.* **2021**, *287*, No. 102330.

(3) Bolouri, P.; Salami, R.; Kouhi, S.; Kordi, M.; Lajayer, B. A.; Hadian, J.; Astatkie, T. Applications of Essential Oils and Plant Extracts in Different Industries. *Molecules* **2022**, *27*, No. 8999.

(4) Aljaafari, M. N.; AlAli, A. O.; Baqais, L.; Alqubaisy, M.; AlAli, M.; Molouki, A.; Ong-Abdullah, J.; Abushelaibi, A.; Lai, K.-S.; Lim, S.-H. E. An Overview of the Potential Therapeutic Applications of Essential Oils. *Molecules* **2021**, *26*, No. 628.

(5) Jugreet, B. S.; Suroowan, S.; Rengasamy, R. R. K.; Mahomoodally, M. F. Chemistry, Bioactivities, Mode of Action and Industrial Applications of Essential Oils. *Trends Food Sci. Technol.* **2020**, *101*, 89−105.

(6) Panda, S.; Sahoo, S.; Tripathy, K.; Singh, Y. D.; Sarma, M. K.; Babu, P. J.; Singh, M. C. Essential Oils and Their Pharmacotherapeutics Applications in Human Diseases. *Adv. Tradit. Med.* **2022**, *22*, 1−15.

(7) Falleh, H.; Ben Jemaa, M.; Saada, M.; Ksouri, R. Essential Oils: A Promising Eco-Friendly Food Preservative. *Food Chem.* **2020**, *330*, No. 127268.

(8) Lucia, A.; Girard, C.; Fanucce, M.; Coviella, C.; Rubio, R. G.; Ortega, F.; Guzmán, E. Development of an Environmentally Friendly Larvicidal Formulation Based on Essential Oil Compound Blend to Control *Aedes Aegypti* Larvae: Correlations between Physicochemical Properties and Insecticidal Activity. *ACS Sustainable Chem. Eng.* **2020**, *8*, 10995−11006.

(9) Lucia, A.; Toloza, A. C.; Guzmán, E.; Ortega, F.; Rubio, R. G. Novel Polymeric Micelles for Insect Pest Control: Encapsulation of Essential Oil Monoterpenes inside a Triblock Copolymer Shell for Head Lice Control. *PeerJ* **2017**, *5*, No. e3171.

(10) Isman, M. B. Commercial Development of Plant Essential Oils and Their Constituents as Active Ingredients in Bioinsecticides. *Phytochem. Rev.* **2020**, *19*, 235−241.

(11) Turek, C.; Stintzing, F. C. Stability of Essential Oils: A Review. *Compr. Rev. Food Sci. Food Saf.* **2013**, *12*, 40−53.

(12) Turek, C.; Stintzing, F. C. Impact of Different Storage Conditions on the Quality of Selected Essential Oils. *Food Res. Int.* **2012**, *46*, 341−353.

(13) Răileanu, M.; Todan, L.; Voicescu, M.; Ciuculescu, C.; Maganu, M. A Way for Improving the Stability of the Essential Oils in an Environmental Friendly Formulation. *Mater. Sci. Eng.: C* **2013**, *33*, 3281−3288.

(14) Tiwari, S.; Singh, B. K.; Dubey, N. K. Encapsulation of Essential Oils - A Booster to Enhance Their Bio-Efficacy as Botanical Preservatives. *J. Sci. Res.* **2020**, *64*, 175−178.

(15) Sundar, S. K.; Parikh, J. K. Advances and Trends in Encapsulation of Essential Oils. *Int.J.. Pharm.* **2023**, *635*, No. 122668.

(16) Lenetha, G. G. A Brief Overview On The Essential Oils' Encapsulation With Biodegradable Polymers. *Nat. Volatiles Essent. Oils* **2022**, *9*, 415−422.

(17) Medeleanu, M. L.; Fărcaş, A. C.; Coman, C.; Leopold, L.; Diaconeasa, Z.; Socaci, S. A. Citrus Essential Oils − Based Nano-Emulsions: Functional Properties and Potential Applications. *Food Chem.: X* **2023**, *20*, No. 100960.

(18) Liang, D.; Wang, C.; Luo, X.; Wang, Z.; Kong, F.; Bi, Y. Preparation, Characterization and Properties of Cinnamon Essential Oil Nano-Emulsion Formed by Different Emulsifiers. *J. Drug Delivery Sci. Technol.* **2023**, *86*, No. 104638.

(19) Sharma, S.; Mulrey, L.; Byrne, M.; Jaiswal, A. K.; Jaiswal, S. Encapsulation of Essential Oils in Nanocarriers for Active Food Packaging. *Foods* **2022**, *11*, No. 2337.

(20) Pavela, R.; Benelli, G.; Pavoni, L.; Bonacucina, G.; Cespi, M.; Cianfaglione, K.; Bajalan, I.; Morshedloo, M. R.; Lupidi, G.; Romano, D.; Canale, A.; Maggi, F. Microemulsions for Delivery of Apiaceae Essential Oils—Towards Highly Effective and Eco-Friendly Mosquito Larvicides? *Ind. Crop Prod.* **2019**, *129*, 631−640.

(21) Bermejo, D. V.; Angelov, I.; Vicente, G.; Stateva, R. P.; García-Risco, M. R.; Reglero, G.; Ibañez, E.; Fornari, T. Extraction of Thymol from Different Varieties of Thyme Plants Using Green Solvents. *J. Sci. Food Agric.* **2015**, *95*, 2901−2907.

(22) Meeran, M. F. N.; Javed, H.; Al Taee, H.; Azimullah, S.; Ojha, S. K. Pharmacological Properties and Molecular Mechanisms of Thymol: Prospects for Its Therapeutic Potential and Pharmaceutical Development. *Front. Pharmacol.* **2017**, *8*, No. 380.

(23) Memar, M. Y.; Raei, P.; Alizadeh, N.; Aghdam, M. A.; Kafil, H. S. Carvacrol and Thymol: Strong Antimicrobial Agents against Resistant Isolates. *Rev. Med. Microbiol.* **2017**, *28*, 63−68.
(24) Sampaio, L. A.; Pina, L. T. S.; Serafini, M. R.; dos Santos Tavares, D.; Guimarães, A. G. Antitumor Effects of Carvacrol and Thymol: A Systematic Review. *Front. Pharmacol.* **2021**, *12*, No. 702487, DOI: 10.3389/fphar.2021.702487.
(25) Zhang, Q.; Fan, K.; Wang, P.; Yu, J.; Liu, R.; Qi, H.; Sun, H.; Cao, Y. Carvacrol Induces the Apoptosis of Pulmonary Artery Smooth Muscle Cells under Hypoxia. *Eur. J. Pharmacol.* **2016**, *770*, 134−146.
(26) Yammine, J.; Gharsallaoui, A.; Fadel, A.; Karam, L.; Ismail, A.; Chihib, N.-E. Encapsulation of Carvacrol and Thymol for a Persistent Removal of Listeria Innocua Biofilms. *J. Drug Delivery Sci. Technol.* **2023**, *84*, No. 104443.
(27) Shlosman, K.; Rein, D. M.; Shemesh, R.; Koifman, N.; Caspi, A.; Cohen, Y. Encapsulation of Thymol and Eugenol Essential Oils Using Unmodified Cellulose: Preparation and Characterization. *Polymers* **2023**, *15*, No. 95.
(28) Zhou, J.; Kong, L. Encapsulation and Retention Profile of Thymol in the Preformed "Empty" V-type Starch Inclusion Complex. *Food Front.* **2023**, *4*, 902−910.
(29) Gutiérrez-González, P.; Fernández-Peña, L.; Lucia, A.; Ortega, F.; Rubio, R. G.; Guzmán, E. Aqueous Dispersions of Oleic Acid Nanodroplets for Thymol Encapsulation. *Colloids Surf., A* **2024**, *690*, No. 133775.
(30) Fernández-Peña, L.; Gutiérrez-Muro, S.; Guzmán, E.; Lucia, A.; Ortega, F.; Rubio, R. G. Oil-In-Water Microemulsions for Thymol Solubilization. *Colloids Interfaces* **2019**, *3*, No. 64.
(31) Mi, D.; Liu, C.; Shi, Q.; Qiao, W. Solubilization of Thymol Based on Alkyl Polyglucoside Microemulsions. *J. Mol. Liq.* **2025**, *417*, No. 126606.
(32) Olukoya, I. A.; Bellmer, D.; Whiteley, J. R.; Aichele, C. P. Evaluation of the Environmental Impacts of Ethanol Production from Sweet Sorghum. *Energy Sustainable Dev.* **2015**, *24*, 1−8.
(33) Alhajj, M. J.; Montero, N.; Yarce, C. J.; Salamanca, C. H. Lecithins from Vegetable, Land, and Marine Animal Sources and Their Potential Applications for Cosmetic, Food, and Pharmaceutical Sectors. *Cosmetics* **2020**, *7*, No. 87.
(34) Anastas, P.; Eghbali, N. Green Chemistry: Principles and Practice. *Chem. Soc. Rev.* **2010**, *39*, 301−312.
(35) Anastas, P. T.; Kirchhoff, M. M. Origins, Current Status, and Future Challenges of Green Chemistry. *Acc. Chem. Res.* **2002**, *35*, 686−694.
(36) Rathod, N. B.; Kulawik, P.; Ozogul, F.; Regenstein, J. M.; Ozogul, Y. Biological Activity of Plant-Based Carvacrol and Thymol and Their Impact on Human Health and Food Quality. *Trends Food Sci. Technol.* **2021**, *116*, 733−748.
(37) Chroho, M.; Rouphael, Y.; Petropoulos, S. A.; Bouissane, L. Carvacrol and Thymol Content Affects the Antioxidant and Antibacterial Activity of Origanum Compactum and Thymus Zygis Essential Oils. *Antibiotics* **2024**, *13*, No. 139.
(38) Soares, A.; Fontes, A. L.; Teixeira, F.; Costa, P.; Pimentel, L.; Pintado, M.; Rodríguez-Alcalá, L. M. Sustainable Synthesis and Optimisation of Ethyl Oleate from High Oleic Acid Waste: A Pathway to Valorise Industrial Byproducts. *Sustainable Food Technol.* **2025**, *3*, 1011−1019.
(39) Wang, X.; Fu, Y.; Washburn, S.; Nguyen, T. B.; Chauhan, A.; Shaikh, S.; Zhao, W.; Wang, H.; Shi, S. Q. Fatty Acid from Recycled Waste Cooking Oil as a Phase-Change Material for Thermal Storage Systems. *RSC Adv.* **2026**, *16*, 5852−5863.
(40) McClements, D. J. Advances in Nanoparticle and Microparticle Delivery Systems for Increasing the Dispersibility, Stability, and Bioactivity of Phytochemicals. *Biotechnol. Adv.* **2020**, *38*, No. 107287.
(41) Gholami-Ahangaran, M.; Ahmadi-Dastgerdi, A.; Azizi, S.; Basiratpour, A.; Zokaei, M.; Derakhshan, M. Thymol and Carvacrol Supplementation in Poultry Health and Performance. *Vet. Med. Sci.* **2022**, *8*, 267−288.
(42) Michiels, J.; Missotten, J.; Van Hoorick, A.; Ovyn, A.; Fremaut, D.; De Smet, S.; Dierick, N. Effects of Dose and Formulation of Carvacrol and Thymol on Bacteria and Some Functional Traits of the Gut in Piglets after Weaning. *Arch. Anim. Nutr.* **2010**, *64*, 136−154.
(43) Costa, M. F.; Durço, A. O.; Rabelo, T. K.; de Souza Siqueira Barreto, R.; Guimarães, A. G. Effects of Carvacrol, Thymol and Essential Oils Containing Such Monoterpenes on Wound Healing: A Systematic Review. *J. Pharm. Pharm.* **2019**, *71*, 141−155.
(44) Guarda, A.; Rubilar, J. F.; Miltz, J.; Galotto, M. J. The Antimicrobial Activity of Microencapsulated Thymol and Carvacrol. *Int. J. Food Microbiol.* **2011**, *146*, 144−150.
(45) Karam, L.; Roustom, R.; Abiad, M. G.; El-Obeid, T.; Savvaidis, I. N. Combined Effects of Thymol, Carvacrol and Packaging on the Shelf-Life of Marinated Chicken. *Int. J. Food Microbiol.* **2019**, *291*, 42−47.
(46) Speranza, B.; Bevilacqua, A.; Campaniello, D.; Altieri, C.; Corbo, M. R.; Sinigaglia, M. Minimal Inhibitory Concentrations of Thymol and Carvacrol: Toward a Unified Statistical Approach to Find Common Trends. *Microorganisms* **2023**, *11*, No. 1774.
(47) Miladi, H.; Zmantar, T.; Chaabouni, Y.; Fedhila, K.; Bakhrouf, A.; Mahdouani, K.; Chaieb, K. Antibacterial and Efflux Pump Inhibitors of Thymol and Carvacrol against Food-Borne Pathogens. *Microb. Pathog.* **2016**, *99*, 95−100.
(48) Khan, S. T.; Khan, M.; Ahmad, J.; Wahab, R.; Abd-Elkader, O. H.; Musarrat, J.; Alkhathlan, H. Z.; Al-Kedhairy, A. A. Thymol and Carvacrol Induce Autolysis, Stress, Growth Inhibition and Reduce the Biofilm Formation by Streptococcus Mutans. *AMB Express* **2017**, *7*, No. 49.
(49) da Silva, B.; do Rosário, D.; Neto, L.; Lelis, C.; Conte-Junior, C. Antioxidant, Antibacterial and Antibiofilm Activity of Nanoemulsion-Based Natural Compound Delivery Systems Compared with Non-Nanoemulsified Versions. *Foods* **2023**, *12*, No. 1901.
(50) Caddeo, C.; Manconi, M.; Cardia, M. C.; Díez-Sales, O.; Fadda, A. M.; Sinico, C. Investigating the Interactions of Resveratrol with Phospholipid Vesicle Bilayer and the Skin: NMR Studies and Confocal Imaging. *Int. J. Pharm.* **2015**, *484*, 138−145.
(51) Pasquali, R. C.; Taurozzi, M. P.; Bregni, C. Some Considerations about the Hydrophilic−Lipophilic Balance System. *Int. J. Pharm.* **2008**, *356*, 44−51.
(52) Singpanna, K.; Charnvanich, D. Effect of the Hydrophilic-Lipophilic Balance Values of Non-Ionic Surfactants on Size and Size Distribution and Stability of Oil/Water Soybean Oil Nanoemulsions. *Thai J. Pharm. Sci.* **2021**, *45*, 487−491.
(53) Zhang, B.; Yang, C.; Liao, S.; Lai, X.; Zhang, Y.; Chen, B.; Xiong, W. Progress on the Synthesis and Applications of the Green Non-Ionic Surfactant Alkyl Polyglycosides. *RSC Adv.* **2025**, *15*, 47333−47359.
(54) Rodríguez-Abreu, C. On the Relationships between the Hydrophilic−Lipophilic Balance and the Nanoarchitecture of Non-ionic Surfactant Systems. *J. Surfactants Deterg.* **2019**, *22*, 1001−1010.
(55) Dari, C.; Si, Y.; Douliez, J.-P.; Tahon, J.-F.; Benezech, T.; Clegg, P. S.; Fameau, A.-L. Mixture of Fatty Alcohols and Alkyl Polyglucosides Stabilizing Water-in-Water Emulsions. *Front. Soft Matter* **2023**, *3*, No. 1328195.
(56) Li, G.; Chen, L.; Ruan, Y.; Guo, Q.; Liao, X.; Zhang, B. Alkyl Polyglycoside: A Green and Efficient Surfactant for Enhancing Heavy Oil Recovery at High-Temperature and High-Salinity Condition. *J. Pet. Explor. Prod. Technol.* **2019**, *9*, 2671−2680.
(57) Fernández-Peña, L.; Guzmán, E.; Ortega, F.; Bureau, L.; Leonforte, F.; Velasco, D.; Rubio, R. G.; Luengo, G. S. Physico-Chemical Study of Polymer Mixtures Formed by a Polycation and a Zwitterionic Copolymer in Aqueous Solution and upon Adsorption onto Negatively Charged Surfaces. *Polymer* **2021**, *217*, No. 123442.
(58) Wang, H.; Jun, Y.; Xiao, X.; Jin, D.; Zhao, N.-J.; Yin, G.-F.; Guo, L.-Q.; Liu, W.-Q. Excitation-Emission Fluorescence Characterization Study of the Three Phenolic Compounds. *Spectrosc. Spectral Anal.* **2010**, *30*, 1271−1274.
(59) Zhang, J.; Wen, J.; Liu, W.-D.; Cui, X.; Chen, Y. Cryo-EM for Nanomaterials: Progress and Perspective. *Sci. China Mater.* **2022**, *65*, 2613−2626.

https://doi.org/10.1021/acssuschemeng.5c13845
ACS Sustainable Chem. Eng. XXXX, XXX, XXX−XXX

(60) Lyu, Z.; Yao, L.; Chen, W.; Kalutantirige, F. C.; Chen, Q. Electron Microscopy Studies of Soft Nanomaterials. *Chem. Rev.* **2023**, *123*, 4051−4145.
(61) Danino, D. Cryo-TEM of Soft Molecular Assemblies. *Curr. Opin. Colloid Interface Sci.* **2012**, *17*, 316−329.
(62) Israelachvili, J. N. *Intermolecular and Surface Forces*; Academic Press: Cambridge, MA, USA, 1989. DOI: 10.1016/C2009-0-21560-1.
(63) Holmberg, K.; Jönsson, B.; Kronberg, B.; Lindman, B. *Surfactants and Polymers in Aqueous Solution*; Wiley: Chirchester, UK, 2002. DOI: 10.1002/0470856424.
(64) Montes, C.; Villaseñor, M. J.; Ríos, Á. Analytical Control of Nanodelivery Lipid-Based Systems for Encapsulation of Nutraceuticals: Achievements and Challenges. *Trends Food Sci. Technol.* **2019**, *90*, 47−62.
(65) Khalid, A.; Arshad, M. U.; Imran, A.; Khalid, S. H.; Shah, M. A. Development, Stabilization, and Characterization of Nanoemulsion of Vitamin D3-Enriched Canola Oil. *Front. Nut.* **2023**, *10*, No. 1205200.
(66) Souza, I. D. L.; Saez, V.; Mansur, C. R. E. Lipid Nanoparticles Containing Coenzyme Q10 for Topical Applications: An Overview of Their Characterization. *Colloids Surf., B* **2023**, *230*, No. 113491.
(67) Pavoni, L.; Perinelli, D. R.; Bonacucina, G.; Cespi, M.; Palmieri, G. F. An Overview of Micro- and Nanoemulsions as Vehicles for Essential Oils: Formulation, Preparation and Stability. *Nanomaterials* **2020**, *10*, No. 135.
(68) Savic, S.; Lukic, M.; Jaksic, I.; Reichl, S.; Tamburic, S.; Müller-Goymann, C. An Alkyl Polyglucoside-Mixed Emulsifier as Stabilizer of Emulsion Systems: The Influence of Colloidal Structure on Emulsions Skin Hydration Potential. *J. Colloid Interface Sci.* **2011**, *358*, 182−191.
(69) Sarheed, O.; Dibi, M.; Ramesh, K. V. R. N. S. Studies on the Effect of Oil and Surfactant on the Formation of Alginate-Based O/W Lidocaine Nanocarriers Using Nanoemulsion Template. *Pharmaceutics* **2020**, *12*, No. 1223.
(70) Fernández-Peña, L.; El Mojahid, B. Z.; Guzmán, E.; Ortega, F.; Rubio, R. G. Performance of Oleic Acid and Soybean Oil in the Preparation of Oil-in-Water Microemulsions for Encapsulating a Highly Hydrophobic Molecule. *Colloids Interfaces* **2021**, *5*, No. 50.
(71) Sauer, M.; Hofkens, J.; Enderlein, J. *Handbook of Fluorescence Spectroscopy and Imaging*; Wiley, 2011 DOI: 10.1002/9783527633500.
(72) Tchaikovskaya, O. N.; Sokolova, I. V.; Kuznetsova, R. T.; Swetlitchnyi, V. A.; Kopylova, T. N.; Mayer, G. V. Fluorescence Investigations of Phenol Phototransformation in Aqueous Solutions. *J. Fluoresc.* **2000**, *10*, 403−408.
(73) Bose, A.; Sengupta, P.; Pal, U.; Senapati, S.; Ahsan, M.; Roy, S.; Das, U.; Sen, K. Encapsulation of Thymol in Cyclodextrin Nano-Cavities: A Multi Spectroscopic and Theoretical Study. *Spectrochim. Acta, Part A* **2019**, *208*, 339−348.
(74) Pan, K.; Chen, H.; Davidson, P. M.; Zhong, Q. Thymol Nanoencapsulated by Sodium Caseinate: Physical and Antilisterial Properties. *J. Agric. Food Chem.* **2014**, *62*, 1649−1657.


CAS BIOFINDER DISCOVERY PLATFORM™
BRIDGE BIOLOGY AND CHEMISTRY FOR FASTER ANSWERS
Analyze target relationships, compound effects, and disease pathways
Explore the platform
CAS
A division of the American Chemical Society

https://doi.org/10.1021/acssuschemeng.5c13845
ACS Sustainable Chem. Eng. XXXX, XXX, XXX−XXX